Received: 10 June 2024 | Revised: 20 November 2024 | Accepted: 3 February 2025

DOI: 10.1002/ecs2.70213

ECOSPHERE
AN ESA OPEN ACCESS JOURNAL

ARTICLE

Special Feature: Insights from Subseasonal Imaging Spectroscopy

Intrinsic dimensionality as a metric for temporal plant diversity evaluation: Case study from the SHIFT campaign

Kerry Cawse-Nicholson[1] | **K. Dana Chadwick**[2] | **Philip G. Brodrick**[3] | **Michael Kiper**[3] | **David R. Thompson**[4] | **David Schimel**[1] | **Charles E. Miller**[1] | **Philip A. Townsend**[1,5] | **Luciana F. Alves**[6] | **Alexey N. Shiklomanov**[7] | **Moses A. Cho**[8,9] | **Abel Ramoelo**[9,10] | **Philemon Tsele**[9] | **Nobuhle Majozi**[8] | **Zoe Amie Pierrat**[1] | **Simon Ferrier**[11]

[1]Carbon Cycle and Ecosystems Group, Jet Propulsion Laboratory, California Institute of Technology, Pasadena, California, USA

[2]Water and Ecosystems Group, Jet Propulsion Laboratory, California Institute of Technology, Pasadena, California, USA

[3]Machine Learning and Instrument Autonomy Group, Jet Propulsion Laboratory, California Institute of Technology, Pasadena, California, USA

[4]Imaging Spectroscopy Group, Jet Propulsion Laboratory, California Institute of Technology, Pasadena, California, USA

[5]Department of Forest and Wildlife Ecology, University of Wisconsin, Madison, Wisconsin, USA

[6]Center for Tropical Research, Institute of the Environment and Sustainability, University of California Los Angeles, Los Angeles, California, USA

[7]NASA Goddard Space Flight Center, Greenbelt, Maryland, USA

[8]Council for Scientific and Industrial Research, Pretoria, South Africa

[9]Department of Geography, Geoinformatics and Meteorology, University of Pretoria, Pretoria, South Africa

[10]Earth Observation Unit, South African National Space Agency, Pretoria, South Africa

[11]CSIRO Environment, The Commonwealth Scientific and Industrial Research Organisation, Canberra, Australian Capital Territory, Australia

Correspondence
Kerry Cawse-Nicholson
Email: kerry-anne.cawse-nicholson@jpl.nasa.gov

Funding information
NASA, Grant/Award Number: 80NSSC21K0086; National Aeronautics and Space Administration; United Nations Educational, Scientific and Cultural Organization (UNESCO); Oak Ridge Associated Universities; National Research Foundation of South Africa (NRF); Jet Propulsion Laboratory; NSF ASCEND Biology Integration Institute (BII), Grant/Award Number: DBI 2021898

Handling Editor: Michelle M. Gierach

Abstract

Current biodiversity metrics derived from remote sensing data are typically applied to small local areas, require significant training data, and are not easily extensible globally. Here we propose the mathematical concept of intrinsic dimensionality (ID) as a method to quantify terrestrial vegetation variability without a need for in situ training data. We apply this technique to airborne imaging spectroscopy data from the Surface Biology and Geology High Frequency Time series (SHIFT) airborne campaign, with weekly overflights from February to May 2022 over a region in California stretching from Figueroa Mountain in the Los Padres National Forest to Point Conception and adjacent coastal areas. ID is considered in both spatial and temporal context—spatial ID represents spectral variability across a geographical region at a single time step, and temporal ID represents spectral variability over time for a single geographical location. Results show an encouraging and significant correlation between spatially calculated ID and in situ vegetation species richness

data despite different spatial scales between the two ($p = 0.01$). Spatial ID remained largely unchanged at each time step over the course of three months during the spring green-up period when vegetation characteristics and spectral responses were changing rapidly (number of species remains unchanged even though spectra reflect phenological change over time). The temporal ID remained constant for pseudo-invariant surfaces such as parking lots, roofs, and rock, but showed increased ID with time for trees, shrubs, and grasses. This robustness of spatial ID to seasonal change is desirable in any measure of species richness because it is insulated from changes in vegetation condition that are unrelated to plant species richness. Even though the spatial ID is consistent across acquisition dates, when considering the full time series (temporal ID), we find that subweekly sampling may be necessary to spectrally capture the full phenological cycle of certain vegetation types.

KEYWORDS
biodiversity, ecological time series, intrinsic dimensionality, Special Feature: Insights from Subseasonal Imaging Spectroscopy, surface biology and geology

INTRODUCTION

Biodiversity is the "variety of life on Earth"—including both species and functional diversity—and this diversity is declining at an alarming rate (United Nations Convention on Biological Diversity, 2020). Reduced diversity results in ecosystems that are less productive and less resistant to perturbations resulting from changing climate, pests, or disease, which in turn can have significant effects on human health (Millennium Ecosystem Assessment, 2005). Imaging spectroscopy has been used to great effect to investigate plant diversity in terrestrial ecosystems. The *spectral variability hypothesis* (SVH) states that species richness will be positively related to variation of spectra in remotely sensed imagery (Palmer et al., 2000), and testing found that spectral variation (in terms of mean distance from spectral centroid) is especially well correlated with the number of rare species (Palmer et al., 2002). Studies on airborne and spaceborne spectral imaging have found empirical relationships between spectral diversity and ecosystem-level in situ plant diversity metrics (Draper et al., 2019; Féret & Asner, 2014; Schmidtlein et al., 2007), and many studies have estimated specific plant structural and functional traits from spectra (e.g., Féret & Asner, 2014; Gholizadeh et al., 2020; Leitão et al., 2019; Schneider et al., 2017; Singh et al., 2015; Wang & Gamon, 2019). In moving from the fine (1–10 m) pixel resolution of airborne sensors—such as the NASA Airborne Visible/Infrared Imaging Spectrometer (AVIRIS)—to the coarser resolution of spaceborne sensors (30–100 m)—such as the upcoming NASA mission to map Earth's Surface Biology and Geology (SBG)—analysis must account for the scale transition from individual plant observations to mixtures of multiple species within a single pixel.

Biodiversity can include taxonomic, phylogenetic, functional, and spectral diversity for vegetation (Cavender-Bares et al., 2020). Some studies consider terrestrial vascular plant species quantified in terms of richness and evenness of spectral "species" (alpha diversity), as in Féret and Asner (2014). Other studies have considered structural diversity using canopy height and foliar density variation (e.g., Schneider et al., 2017), or functional diversity using foliar chemical and morphological traits (e.g., Singh et al., 2015). Yet others consider the turnover of composition across space (beta diversity; Draper et al., 2019; Leitão et al., 2019), or regional diversity (gamma diversity, which is the diversity across an entire ecosystem or region). Some definitions of biodiversity are centered around insect and/or mammal abundance and variability (Wang & Gamon, 2019). In this study, we focus specifically on canopy emergent plant diversity (i.e., plant species observable from above), which is distinct from overall biodiversity in an ecosystem but a major driver thereof because of the critical role plants play as primary producers, as regulators of water and energy fluxes, and as providers of habitat (Schimel et al., 2013).

Remote sensing observations of ecosystems, particularly those collected by spaceborne sensors, typically contain mixtures of plant species, and these mixtures must be understood in order to estimate species diversity. Methods for unmixing mixed pixels into their base components or "endmembers" have been developed,

although many rely on a known library of spectra and provide abundances of these spectra in each pixel (e.g., Roberts et al., 1998, and other spectral mixture analysis algorithms as reviewed in Somers et al., 2011). These algorithms generally use cost functions driven by overall spectral variance, instead of carefully defined spectral features, and can be severely hampered by endmember collinearity. This results in poor modeling of low amplitude but physically meaningful absorption features (Sousa et al., 2022). Supervised unmixing algorithms also depend on the representativeness of the input library and may not account for within-class variability (Somers et al., 2011). This will be especially problematic for highly diverse, poorly spectrally sampled regions in the world. To address this issue, we propose a method that accounts for subpixel unmixing and does not rely on in situ training data for mapping vegetation variability. We produce spatial maps of spectral variability by considering 1 km × 1 km grid cells (approximately 200 pixels × 200 pixels, hereafter referred to as cells) and independently calculating the diversity metric per cell. This approach for characterizing ecosystem diversity will be important to fully exploit the growing catalog of global imaging spectroscopy data from missions like EnMAP (Storch et al., 2023), PRISMA (Cogliati et al., 2021) and EMIT (Thompson et al., 2024). This will also be critical for the next generation of orbital spectrometers, such as the SBG mission (Cawse-Nicholson et al., 2021), which will provide global coverage at biweekly cadence. These missions promise powerful new insight into the biodiversity of our changing ecosystems but require an analytical framework to map this diversity at orbital resolutions in a consistent manner across space and time.

We propose a mathematical metric called "intrinsic dimensionality" as a proxy for vegetation variability in the form of species richness. The intrinsic dimensionality (ID) of an image can be defined as the dimension of the linear signal subspace or the number of linearly separable and spectrally distinct signal sources within a spectral image or subimage (Cawse-Nicholson et al., 2019; Cawse-Nicholson, Damelin, et al., 2013). The independent spectral signals combine to form the measured spectrum of each pixel. While nonlinear unmixing techniques have been proposed (see Heylen et al., 2014 for a review), here we assume linear mixing, where nonlinear interactions such as multiple scattering in plant canopies are often detected as an additional "dimension". In the context of vegetation, the pure signals indicate different canopy optical properties. More generally, they indicate the plant's unique functional niche of chemistry and structure in the ecosystem. By enumerating these signals, ID offers a path to measure vegetation variability without training data, based only on the loose assumption of linear mixing within pixels. This technique has been applied to airborne imaging spectroscopy data in previous studies where ID values ranging from ~20 to ~40 were observed (Cawse-Nicholson et al., 2019; Cawse-Nicholson, Damelin, et al., 2013; Thompson et al., 2017). Note that spectral variation of individuals within a species due to differing nutrient levels, phenology, vegetation health, etc. (i.e., functional diversity) that exceeds the noise level will increase the ID. This differentiation is important in measuring the vegetation variability of the region, and we consider this a model strength. Ancillary data, such as vegetation phenology, can be used in addition to the ID to quantify the impact of phenological variation. ID has been demonstrated to be accurate in differentiating surface minerals, is mathematically sound, and outperforms simple clustering (Cawse-Nicholson et al., 2019; Cawse-Nicholson, Damelin, et al., 2013). There is great advantage in pursuing a diversity metric that is generalizable and does not rely on local training data.

In this manuscript, we evaluate the potential of ID for mapping vegetation variability. To do this, we first provide an overview of ID; next, we detail the SHIFT airborne campaign and associated fieldwork; we demonstrate the relationship between ID and in situ species counts; and finally, we quantify the gain in information content due to frequent temporal sampling of spectral data.

DATA

The NASA Jet Propulsion Laboratory (JPL), along with The Nature Conservancy's Point Conception Institute and the University of California at Santa Barbara (UCSB) launched the SBG High-Frequency Time Series (SHIFT) campaign (Brodrick et al., 2023; Chadwick et al., 2025) as an airborne precursor campaign to NASA's upcoming SBG mission. As part of the Earth System Observatory, SBG will include: (1) an imaging spectrometer covering the range 400–2500 nm with 10-nm spectral sampling, 30-m spatial sampling, and 16-day revisit; and (2) a multiband thermal instrument with 60-m ground sampling and a three-day revisit, acquiring data in two visible-to-near-infrared channels, two midwave infrared channels, and six thermal channels in the 8–12 μm range (Cawse-Nicholson et al., 2021; Stavros et al., 2023). The airborne data from SHIFT has been used to determine the optimal design for the imaging spectrometer by simulating various spatial, spectral, and temporal resolutions (Cawse-Nicholson et al., 2023). The SHIFT campaign included airborne and field data that covered more than 1600 km^2 with an elevation change of ~1200 m within Santa Barbara County, California, and includes the Santa Ynez Valley, the Los Padres National Forest, The Nature

Conservancy's Jack and Laura Dangermond Preserve, UCSB's Sedgwick Reserve, and the Point Conception Marine Reserve Area. This region is highly biodiverse, including shrublands, grasslands, and agricultural regions, making it an ideal test location to understand how rapidly ecosystems change within a season.

Airborne data

AVIRIS-NG, the Next Generation AVIRIS, is an airborne instrument operating in the visible to shortwave infrared region (from 380 to 2510 nm) with 5 nm spectral sampling. AVIRIS-NG data acquired for SHIFT has 5-m spatial sampling, with flight altitude approximately 5 km above ground level. We used the surface reflectance product produced by the AVIRIS team (Brodrick et al., 2023), which uses the ISOFIT atmospheric correction algorithm (Thompson et al., 2018). We then removed bands where deep water vapor absorptions obscure the surface (we used bands in the wavelength ranges [405, 1340 nm], [1460, 1800 nm], and [2050, 2450 nm]). Flights were acquired approximately weekly on the following dates in 2022: February 24, 28, March 8, 16, 22, April 5, 12, 20, 29, and May 3, 11, 17, 29 (for more information see Brodrick et al., 2023; Chadwick et al., 2025). In this Mediterranean ecosystem, multispectral satellite data showed routinely high rates of phenological change during this period, while also having low cloud cover (Chadwick et al., 2025). Figure 1 shows the flight lines acquired on 24 February; the same pattern was repeated on subsequent sorties.

Field data

Field teams collected a variety of spectral and biological parameters from 315 sites within the SHIFT study area. Each site was approximately 8 m × 8 m, and the locations were subjectively determined to cover a range of plant functional types, climate, topography, geology, and land use (Chadwick et al., 2025; Queally et al., 2024). Every plant species with spatial coverage ≥1% was identified within each site along with its fractional cover

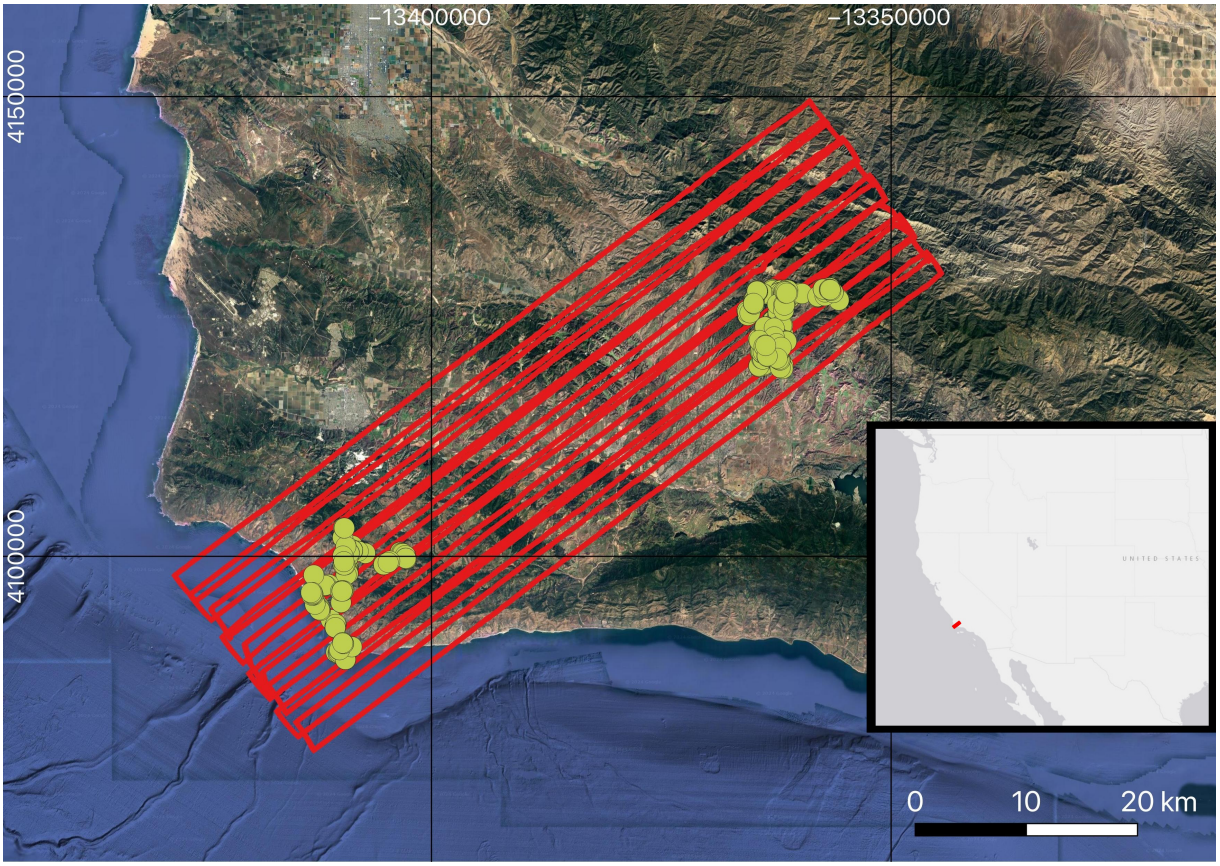

FIGURE 1 Airborne Visible/Infrared Imaging Spectrometer (AVIRIS)-next generation (NG) flight lines acquired on February 24, 2022 (red boxes) and the locations of the field sites (yellow circles). The grid shows the location in Universal Transverse Mercator (UTM) coordinates in Zone 10 S. The inset image shows the site location along the California coast using the ESRI basemap.

(determined visually by field teams and provided in classes: <1%; 1%–10%; 10%–25%; 25%–50%; 50%–75%; 75%–100%). A total of 254 unique plant species were recorded during the field campaign, with an average of 8 species (range 1–19) per plot in grasslands and an average of 4.2 (range 1–15) per plot in shrublands. Field observations were recorded between February and September 2022 and continued past the end of the flight campaign (May 29, 2022). We used all field data in our comparison, as the number of species was unlikely to change over the course of only 4 months. Further details of the campaign design and field sampling methodology are provided by Chadwick et al. (2025).

Two metrics for in situ diversity were used. First, we compared the ID to the number of dominant (>25% fractional cover) species in each site. For a full assessment of different thresholds, see Appendix S3. Second, we calculated the inverse Simpson concentration index (Chao et al., 2014; Rossi & Gholizadeh, 2023; Simpson, 1949) for each site, or group of sites within our region of interest. For each fractional class, we assigned a weight representing the lower value of the class, for example, a plant species recorded as having fractional cover of 10%–25% would be assigned a weight of 0.1, a plant species recorded as having fractional cover of 25%–50% would be assigned a weight of 0.25, etc. The resulting weights of all species are then normalized so that their sum equals one. The inverse Simpson concentration index, SI, is then defined as:

$$\mathrm{SI}_l = 1/\sum_{i=1}^{m} w_i^2, \tag{1}$$

where w_i represents the normalized weight (fractional abundance) of each tree species, for i species present at site l. Note that ID is a metric of vegetation variability, which could also include intra-species variability (e.g., healthy and unhealthy plants of the same species which would have very different spectral responses). Thus, the in situ species richness is not entirely equivalent to ID, but this fieldwork provides a useful comparison in the larger context of biodiversity.

METHODS

We consider ID in both spatial and temporal contexts—spatial ID represents spectral variability across a geographical region at a single time step, and temporal ID represents spectral variability over time for a single geographical location.

Spatial intrinsic dimensionality

Measuring the spatial ID from real data requires variability in the environment to be distinguished from variability due to measurement noise or nonsignal artifacts. We use Random Matrix Theory (RMT) to quantify ID (Cawse-Nicholson, Damelin, et al., 2013). If a matrix X represents the observed spectral image with n pixels × p spectral channels, then the observation covariance matrix is given by $S = X^T X$ (assuming scaling and centering), where X^T represents the transpose of matrix X. We assume that the image may be represented as a linear combination of signal and nonsignal, such that $X = Y + \varepsilon$, where Y is the truth and $\widetilde{\varepsilon} \setminus \mathrm{mathcal}\{\mathrm{N}\}\,(0, \Sigma)$, with Σ defined as the noise covariance matrix. The eigenvalues of the image covariance matrix can be compared with the eigenvalues of the noise covariance to determine the number of detectable spectral signals in the image, or the ID. More detail may be found in Cawse-Nicholson, Damelin, et al. (2013).

An eigenvalue λ_k is regarded as signal if,

$$\lambda_k > \rho_k\, c(N,p), \tag{2}$$

$$\rho_k = \frac{{e_\Pi^k}^T \Sigma\, e_S^k}{{e_\Pi^k}^T e_S^k}, \tag{3}$$

where $\Pi = S - \Sigma$, and e_Π^k and e_S^k are the kth eigenvectors of Π and S, respectively. The constant c depends on the number of pixels and the number of channels and is given in (Cawse-Nicholson, Damelin, et al., 2013). This equation assumes that $N, p \to \infty$. In practice, the equation holds with $N > 500$ and $p > 100$ (Cawse-Nicholson et al., 2022). ID is inherently dependent on the appropriate construction of a noise matrix, which is outlined in *Noise estimation*.

When processing the SHIFT data, we used the 5-m mosaic of all flight lines, made available one acquisition day at a time. A coarser grid is used for spatial ID by considering 1 km × 1 km grid cells (approximately 200 pixels × 200 pixels, hereafter referred to as cells) and independently calculating the ID per cell. Each cell had a total of 40,000 pixels and 335 spectral bands, meeting the ID requirements for N and p. Smaller cell sizes were investigated but did not significantly change the overall spatial patterns.

Temporal intrinsic dimensionality

In *Spatial Intrinsic Dimensionality*, we calculated spatial ID independently for each time step to study the spatial

patterns (image size [n_S pixels, p spectral channels]) where the n_S pixels are all located within a contiguous spatial area or grid cell for a single observation time. To study temporal ID, we calculated a second set of ID metrics on image cubes concatenated through time (image size [(n_T pixels × T timesteps), p spectral channels]). Here, the n_T pixels are not geographical neighbors but instead represent a single class—for example, consider the matrix with rows representing n_T tree pixels for all observation times, and columns representing the spectral characteristics for each pixel. Spatial ID can be used to estimate species richness, but evaluating temporal ID can be complementary and used to understand the increase in information content over time due to phenological change (Cawse-Nicholson et al., 2023). The primary goal of SHIFT was to determine the frequency with which rapidly changing ecosystems should be sampled, by considering a region with low cloud frequency and high phenological change over a short time period (Chadwick et al., 2025). Temporal pixel stacks can be created by combining pixel $x_{i,t0}$ at location i and time $t0$, with pixel $x_{i,t1}$ at the same location i and time $t1$, to create $\widetilde{x}_i = [x_{i,t0}, x_{i,t1}]$. In environments that change very little over time (e.g., bare surfaces), the spectra should remain unchanged within the noise levels, and the ID of the concatenated set should be the same as the ID of each time step considered individually, as no new endmembers (information) have been added (i.e., the rank of the image covariance matrix remains unchanged). Thus, the change in temporal ID serves as a proxy for overall spectral change seen at each time step.

To evaluate this, we selected specific land cover classes within the image to track over time. Each set was chosen to provide a wide range of temporal ID changes, with each material abundant enough to obtain a measure of its spatial ID. In total, the six selected sets were: tree, chaparral/shrub, grassland, flat rooftops, parking lot asphalt, and rock outcrops, with the number of pixels and representative area given in Table 1. Pixels from each set were manually extracted, and the same pixel locations were followed throughout the campaign.

TABLE 1 Pixel quantities for each of the six land cover classes used to analyze the temporal intrinsic dimensionality.

Land cover class	Spatial pixel count	Area (m^2)
Rock outcrop	2054	61,620
Tree	1028	30,840
Parking lot asphalt	537	16,110
Grass	405	12,150
Flat rooftop	349	10,470
Chaparral/shrub	342	10,260

All pixel locations were selected within an internal boundary (i.e., no tree canopy edges, no rock outcrop edges, no roof edges). The rock pixels were selected from very large solid rock formations, such that each rock identified was a solid mass, and visual spectral analysis confirmed no vegetation. Similarly, the center points of large tree crowns were selected to minimize mixtures where possible. The chaparral/shrub class included general low-lying vegetation and may include some mixtures due to the spatial resolution of the image. Higher resolution images within Google Earth were used to confirm labels, and visual spectral analysis was used to remove any class outliers.

These classes serve as a proxy for the range of possible temporal ID changes in the scene. The parking lot and flat rooftop regions are hypothesized to be more likely to be invariant to periodic or cyclical material changes (low temporal ID over the 3-month period) compared with the vegetative areas, which are more sensitive to environmental factors leading to greater degrees of biochemical and thus spectral changes over a shorter time window (high temporal ID over the 3-month period).

Noise estimation

The ID equations given in (2) and (3) are simple and easy to implement, given only two inputs—the image and an estimate of noise. However, the noise covariance matrix Σ can be difficult to compute accurately. Here the signal is the "true" surface reflectance, that is, the hemispherical-directional reflectance factor integrated across the 5-m sampled pixel (Thompson et al., 2018). We define "noise" as any other contributions to the estimated reflectance—including photon shot noise, dark current, calibration uncertainty, adjacency effects, sun-sensor geometry artifacts, bi-directional reflectance distribution, residual atmospheric effects, sensor artifacts, etc. Such changes could modify the hemispherical directional reflectance, that is, the directional quantity observed from the sensor perspective, even if the objects under observation are the same (imagine looking at shaded and sunlit sides of a tree canopy, which would each represent a different noise value within the respective pixel observations). To maintain consistency with past literature, we will continue to refer to ε as "noise" but note that it includes all nonsignal contributors to the observable. While this "nonsignal" term may not be Gaussian in practice, this is a common assumption that is typically used when estimating ID and we will maintain the assumption of Gaussian noise in this manuscript (Bioucas-Dias & Nascimento, 2008a; Cawse-Nicholson, Damelin, et al., 2013; Robin et al., 2015; and others).

Several methods have been proposed to estimate this noise. Simple methods for estimating independent and identically distributed (i.i.d.) noise—where the noise has the same variance in every spectral band—approximate the noise directly from the eigenvalues of the image covariance matrix (Kritchman & Nadler, 2009). However, imaging spectrometers rarely have the same noise levels for every band. Spatial methods such as that proposed by Meer et al. (1990) divide the image into progressively smaller blocks in order to identify homogenous regions, whereby the standard deviation of a such a region would represent the noise. However, the noise is calculated independently in each band, neglecting the potential for inter-band noise correlation. Bioucas-Dias and Nascimento (2008a, 2008b) proposed a noise estimation regression technique that has been tested on AVIRIS classic imagery and has performed well (Cawse-Nicholson, Damelin, et al., 2013). If we assume that the signal between neighboring bands is correlated but noise is not, then we could remove a band, and use the other bands to predict its value, and the difference between the predicted and observed values can be considered noise. However, AVIRIS-NG is a pushbroom spectrometer (as opposed to AVIRIS classic which is a whiskbroom instrument) with much finer band spacing (5 vs. 10 nm). This results in spectrally correlated noise, which results in an underestimation of the noise when using regression techniques (Cawse-Nicholson, Robin, & Sears, 2013; Robin et al., 2015), and nonrandom effects (such as minor calibration offsets between pushbroom detectors) will not be characterized as noise.

ID is particularly sensitive to the underestimation of noise, which leads to significant overestimation of ID, often approaching its maximum value (the number of spectral bands). To better characterize the nonsignal term in high-spectral-resolution pushbroom data, we assume that

$$\varepsilon = (a \times \widehat{\varepsilon}) + b, \tag{4}$$

where $\widehat{\varepsilon}$ is determined using the traditional regression technique described by Bioucas-Dias and Nascimento (2008a, 2008b) and a and b are constants. To estimate these constants, we chose ten 101 pixel × 101 pixel subsets X_i within an AVIRIS-NG flight line (the subset size was selected for computational efficiency, and larger subsets did not yield significantly different results). We found that the ID of the concatenation $[X_i, X_i]$ was larger than the ID of X_i for $a = 1$ and $b = 0$, which cannot be true since no extra information was added; only the number of pixels changed. Prior simulations had shown that when noise is known, RMT is insensitive to the number of pixels for $N > 500$ (Cawse-Nicholson et al., 2022). We iteratively increased both constants until we obtained a consistent value of the ID for the original subset as well as the duplicate concatenations and found a solution at $a = 10$ and $b = 0$. This was true for multiple subsets in all flight lines used. This technique allowed us to produce a full noise covariance matrix at a high enough amplitude to maintain expected RMT performance.

Validation

Scale is an important consideration for our validation. Trees might have a crown diameter of ~10 m, but grasses have leaves ~1 cm. Subpixel spectral effects—including defense compound absorption features—should be captured in the ID estimation with an appropriate noise matrix selection. The eigenvectors obtained by an ID estimate have no prescription of physical length scale (the size of the scene constituents relative to the spatial resolution of the image); they simply represent the complete basis that can reconstruct the complete range of observed spectra. In some cases, this may mean that subpixel features are individual components. In others, dominant pixel-level or super-pixel-level spectral characteristics will be captured. The variability and mixing level within a subset of pixels determine the matrix decomposition, which means that spatial ID may capture inter- and intra-species differences. However, there is a limitation on the detection of low-abundance end members. If an end member is so (spatially or spectrally) small that its contribution to the overall observed spectrum is below the noise levels, then that end member will not count towards the ID.

The standard 1 km × 1 km grid used to create our spatial ID map was not appropriate for validation since it is so much larger than the field plots, which covered only 8 m × 8 m for a single plot. Therefore, to validate our results, we extracted a set of 100 m × 100 m cells centered around each field plot and computed the ID. We then compared the spatial ID to field estimates of species richness—the integer number of unique species present, regardless of the number of individuals identified at each plot—for each species that covered more than 25% of the site area (i.e., more than 16 m^2 of field cover for an 8 m × 8 m site, which was evaluated against a set of airborne image pixels where each pixel covers 25 m^2). However, the plot locations were not identified with this spatial ID comparison in mind, and often did not fully sample all species present in the much larger spatial ID cell. Figure 2 shows three plots that were recorded as predominantly single species, whereas the aerial image over the ID cell shows clear variability in the landscape, and so we would expect the spatial ID for the grid cell to be higher than one

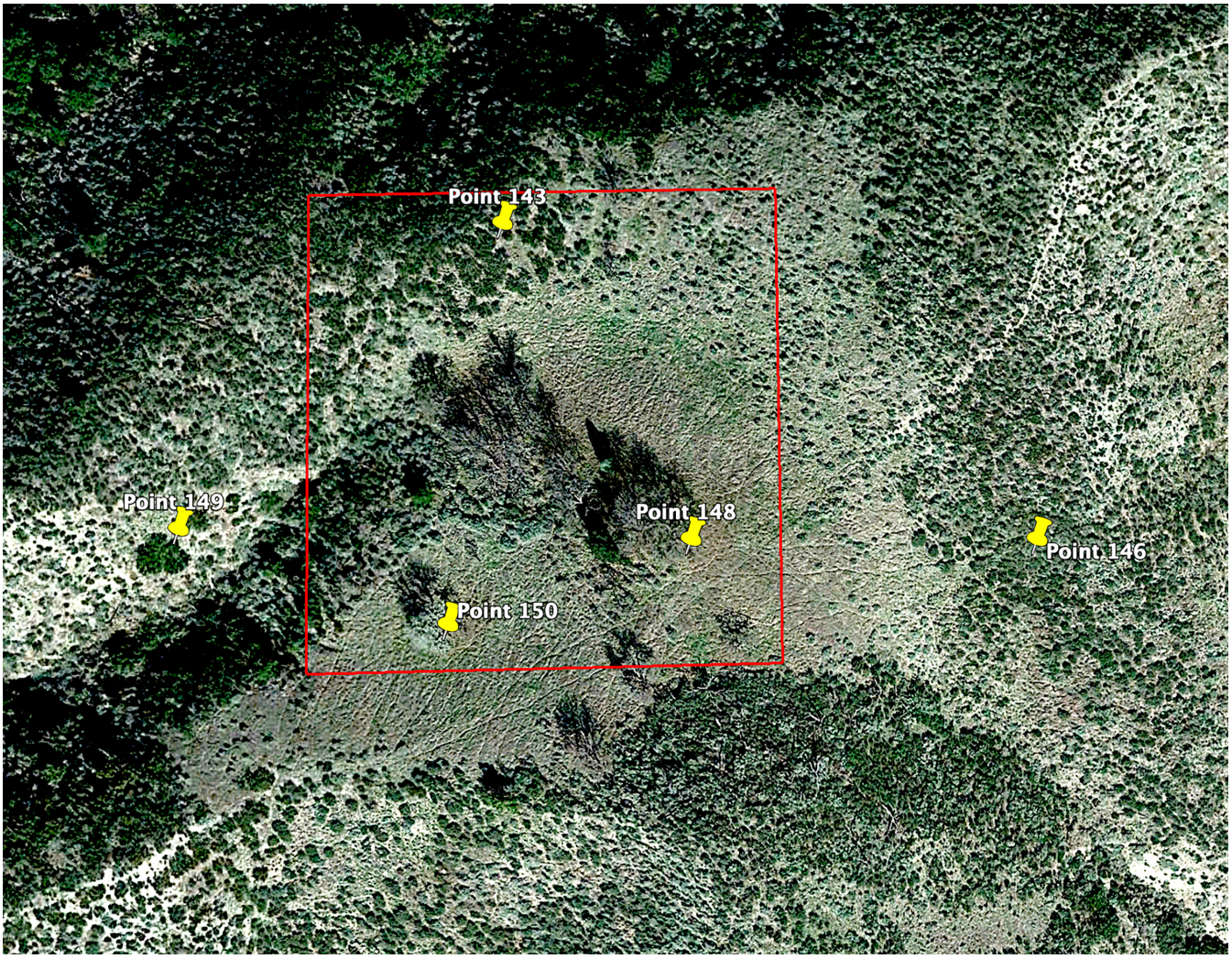

FIGURE 2 Three field plots—Points 143, 148, and 150, each recorded as containing only a single species with >10% abundance. The red box illustrates a potential 100 m × 100 m grid cell. There are clearly more species contained in the larger 100 m × 100 m cell, and so it is beneficial to consider grid cells with multiple field sites contained within. The background is obtained from Google Earth.

based on visual inspection. Since the plot sizes are significantly smaller than the spatial ID cell size and several plots may fall within a single cell (see Figure 2), we merged the species that exceeded 25% coverage in all plots within 40 m of each cell center (since each field plot is 8 m × 8 m, this means that the full neighboring plot sites were contained within our 100 m × 100 m cell). This merging also accounted for multiple revisits of the same plot, so the union of all dominant species observed at a single plot would be used. For this reason, we disregarded species labeled "NPV" (nonphotosynthetically active vegetation), since this could include a number of different species that may become identifiable later in the season. This gave us a useful indication of field diversity visible from an airborne spectrometer to determine the value of ID as a vegetation variability metric. We used the coefficient of determination (R^2) as the metric of performance.

RESULTS

Figure 3 shows the map of spatial ID over the SHIFT domain for a single time step acquired at the beginning of spring. The ocean has a relatively low ID (~5) and the developed region has a relatively high spatial ID (>20). This is in line with a previous work that showed higher spatial ID over developed regions and managed landscapes (Asner et al., 2012; Thompson et al., 2017). Developed regions may include spectral properties from vegetation as well as buildings, roads, and other manufactured surfaces.

Appendix S1 shows the spatial ID maps for all acquisition dates, but there is not much change between them. To illustrate this, for each cell, we have computed a linear regression and plotted the slope. Figure 4 shows a very small slope for all cells, with some negative change along the coastline that is likely indicative of tidal

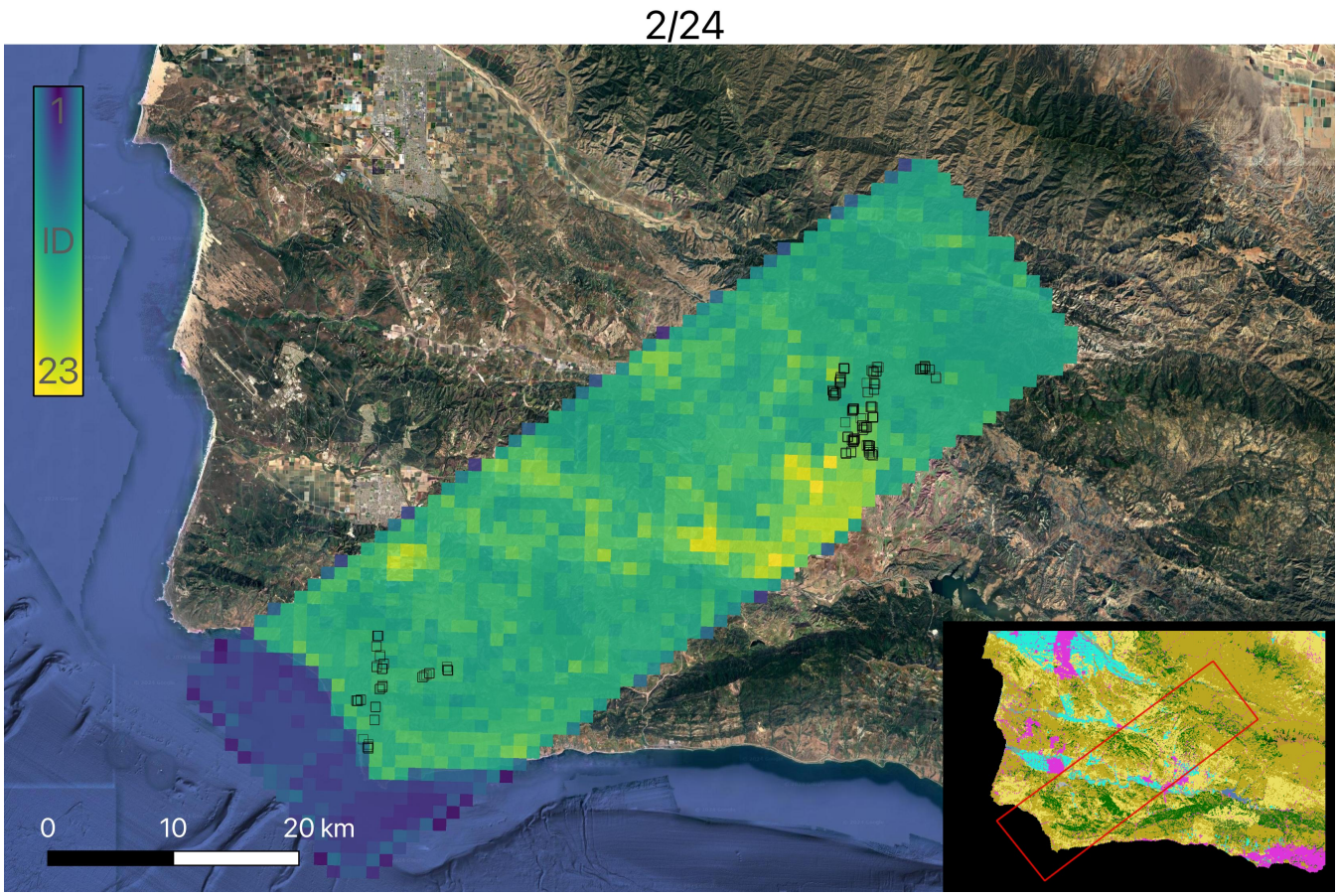

FIGURE 3 The intrinsic dimensionality (ID) of the SHIFT mosaic acquired on February 24, 2022. The ocean has lower ID (~5), and the developed/agricultural regions have the highest ID (>20). Field sites are overlain in black squares. Low ID values around the edges of the flight lines are due to fewer pixels and zero padding within the outer cells. The inset shows the National Landcover Database over the same region, where pink is developed land, green is forest, tan is shrub/scrub, yellow is herbaceous, and cyan is cultivated crops (United States Geological Survey, 2021; note that this has been recolored from the conventional classification to aid with differentiation between colors).

changes. The largest relative change in ID is in the ocean, as shown for a sample pixel in Figure 5. This contrasts with the significant spectral change shown in field and airborne spectra over land for the same timeframe by Chadwick et al. (2025).

In Figure 6, the evaluation of temporal ID shows that classes such as rock, roof, and parking lot remain largely unchanged throughout the campaign, which is to be expected. Grasslands also did not show additional temporal dimensionality beyond ~monthly revisit. Shrubs reached the optimal temporal ID with ~10-day repeat observations, but the observed trees changed so rapidly that they may benefit from subweekly observations. The temporal ID change could reflect a variety in phenological leaf flush patterns across both individual trees and different species, as well as changing dynamics in the understory.

Figure 7 shows the comparison of the number of species recorded in field plots that had over 25% cover with the spatial ID. While spatial ID is a relatively weak predictor of number of dominant species ($R^2 = 0.26$), this is still an encouraging comparison given the difference in spatial scales (significance p value $= 0.01$). Recall that each field site is only 8 m × 8 m, but an ID window of at least 100 m × 100 m was required to satisfy the model assumptions. Figure 7 shows that the spatial ID of the image window is always greater than the number of dominant species observed in the field. This is because the spatial ID cell is so much larger than a field plot, and also because spatial ID will detect variation not recorded in the field survey, such as heterogeneous soil types. Appendix S2 shows the impact of spatial ID cell size and the validation considering spatial ID windows with a limited number of field samples contained within.

DISCUSSION

In this study, we found an encouraging relationship between ID and the number of plant species that have >25% aerial cover when comparing 100 m × 100 m

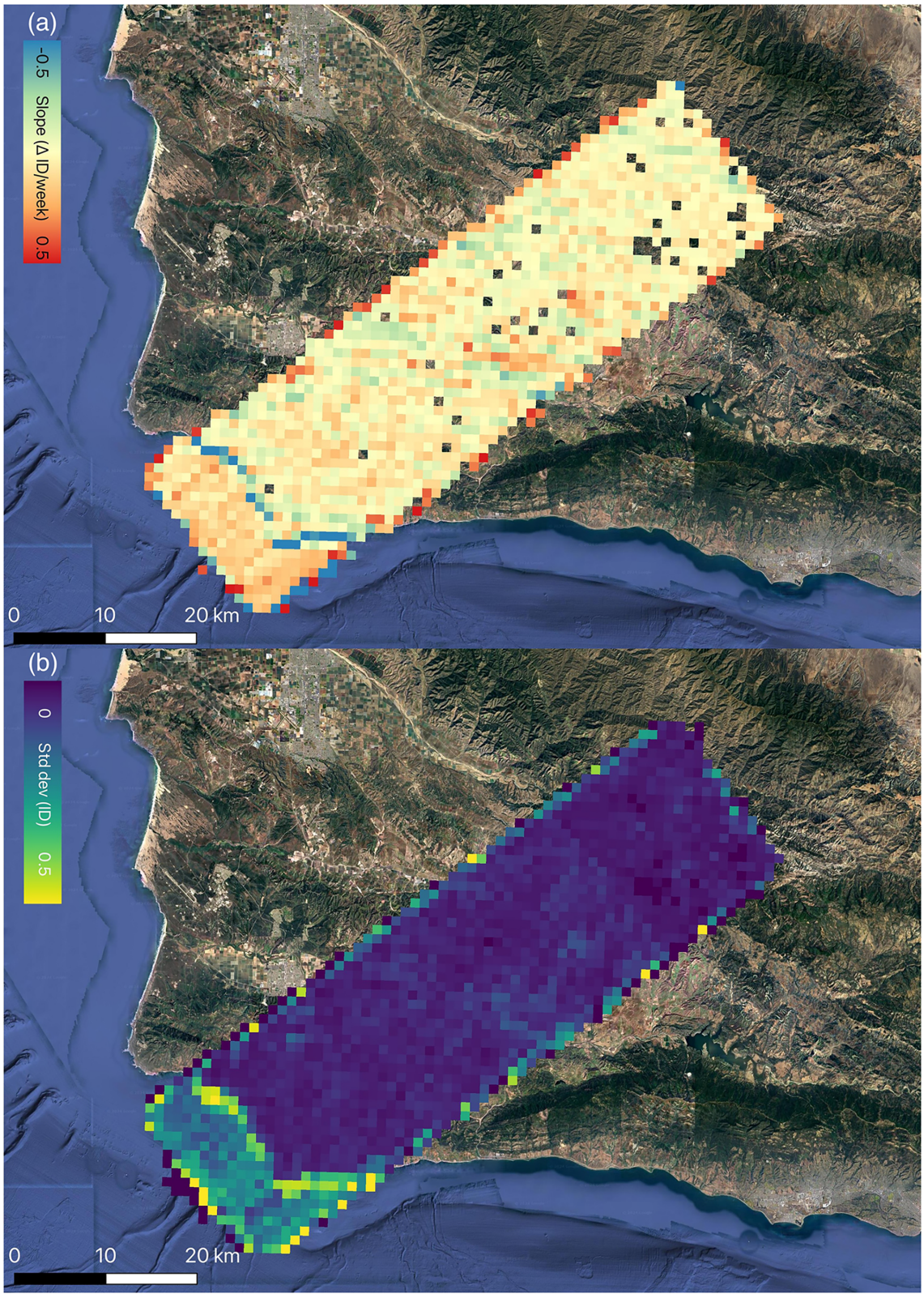

FIGURE 4 The (a) regression slope and (b) mean-normalized SD of the spatial intrinsic dimensionality (ID) estimates over time. The decrease in spatial ID along the coastline most likely points to tidal or glint changes. The rest of the image shows very little significant change in ID over our three-month sampling period. Anomalous slope values around the edges of the flight lines are due to small differences in flight line extents, and fewer pixels and zero padding within the outer cells.

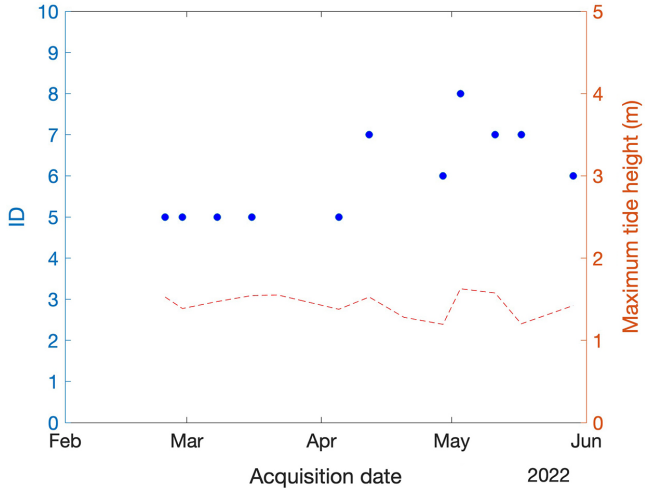

FIGURE 5 The spatial intrinsic dimensionality (ID) for a sample grid cell in the ocean. After April 12, the ID increases slightly. For context, the maximum morning tide height is also shown for nearby Santa Barbara. *Source*: https://tidesandcurrents.noaa.gov/.

remote sensing data to 8 m × 8 m field sites (Figure 7), illustrating the potential of spatial ID as a metric for vegetation variability. We find this promising result even though the spatial scale of fieldwork was several orders of magnitude smaller than the spatial ID cells (64 vs. 10,000 m^2) and the field species richness did not capture potential intra-species classes that might be captured by ID (such as healthy and unhealthy plants of the same species). Palmer et al. (2002) noted that the SVH was likely to apply to larger spatial scales (1–1000 ha). Rocchini et al. (2007) also stressed the importance of both spatial and spectral scales when considering SVH.

Some studies have used multispectral data to estimate plant diversity. For example, Madonsela et al. (2017, 2018, 2021) used Landsat-8 multispectral data or various spectral indices to predict α-diversity with R^2 values ranging between ~0.2 and ~0.4 for 30-m remote sensing data compared with field plots equivalent to ~9 pixels. Rocchini et al. (2007) found good correlations between species richness in 100-m^2 plots for Quickbird, ASTER, and Landsat ETM+ (i.e., $r = 0.69$, $r = 0.43$, $r = 0.67$, respectively). Imaging spectroscopy is expected to better predict diversity due to the improved ability to discriminate between plant chemistry and functional traits using the continuous spectrum rather than discrete spectral bands. Féret and Asner (2014) predicted α-diversity with an R^2 of 0.74 using airborne imaging spectroscopy data with 2-m spatial sampling and field sites equivalent to ~350 pixels. In contrast, our study used airborne imaging spectroscopy data with 5-m spatial sampling, and field plots equivalent to <2 pixel. However, spatial ID has the advantage of being globally applicable with no training requirement and can be used on satellite-scale data (30–100 m spatial sampling) without requiring the detection of individual crowns. This method is also independent of the ecosystem sampled. While the ID maps in Figure 3 were produced at 1 km cell size (200 × 200 pixels in each cell), the validation was done at 100-m cell size (20 × 20 pixels). Therefore, it would be feasible to produce ID maps at a subkilometer scale for future missions with 30 m proposed spatial sampling, such as SBG.

Future studies will include a validation with larger fieldwork plots. We will also consider different ways to represent the field diversity for comparison. Since spatial ID must account for all contributions to the observed spectra regardless of length scale, we compared spatial ID to dominant species richness and the inverse Simpson concentration index. For spectral images with more continuous spatial variability, it may be appropriate to consider other representations of the observed diversity such as Shannon's index (Shannon, 1948), which considers both species richness and abundance (evenness). This may also better capture plots with greater *intra*-specific trait variation (Bolnick et al., 2011; Violle et al., 2012). This is especially relevant for traits that directly influence the species' reflectance, such as water content, pigments, and leaf/canopy structure (e.g., Helsen et al., 2021) since these properties are likely to increase the spatial ID relative to the number of species. Future work might evaluate the extent to which spectral ID analysis can capture known patterns of intraspecific trait variation in California grasses in response to variations in temperature and water availability (Sandel et al., 2021). The ID of a scene can also only capture features represented in the reflectance, and many species present similar or nearly identical reflectance characteristics. As such, comparisons to functional diversity metrics may also prove fruitful at the global scale.

Spatial ID remained largely unchanged over the course of three months during the spring green-up period when other vegetation metrics (such as greenness or foliar traits) were changing rapidly (Chadwick et al., 2025). This robustness to seasonal change is likely because the number of physical "endmembers" remains unchanged. If τ plant species are present but senesced, the spatial ID will be the same as τ plant species in full-leaf conditions, even though the spectra themselves may be different between the two time points. This property is desirable in any measure of species richness because it is robust against changes in vegetation conditions that are unrelated to intrusion or elimination of particular species (unless of course one species entirely

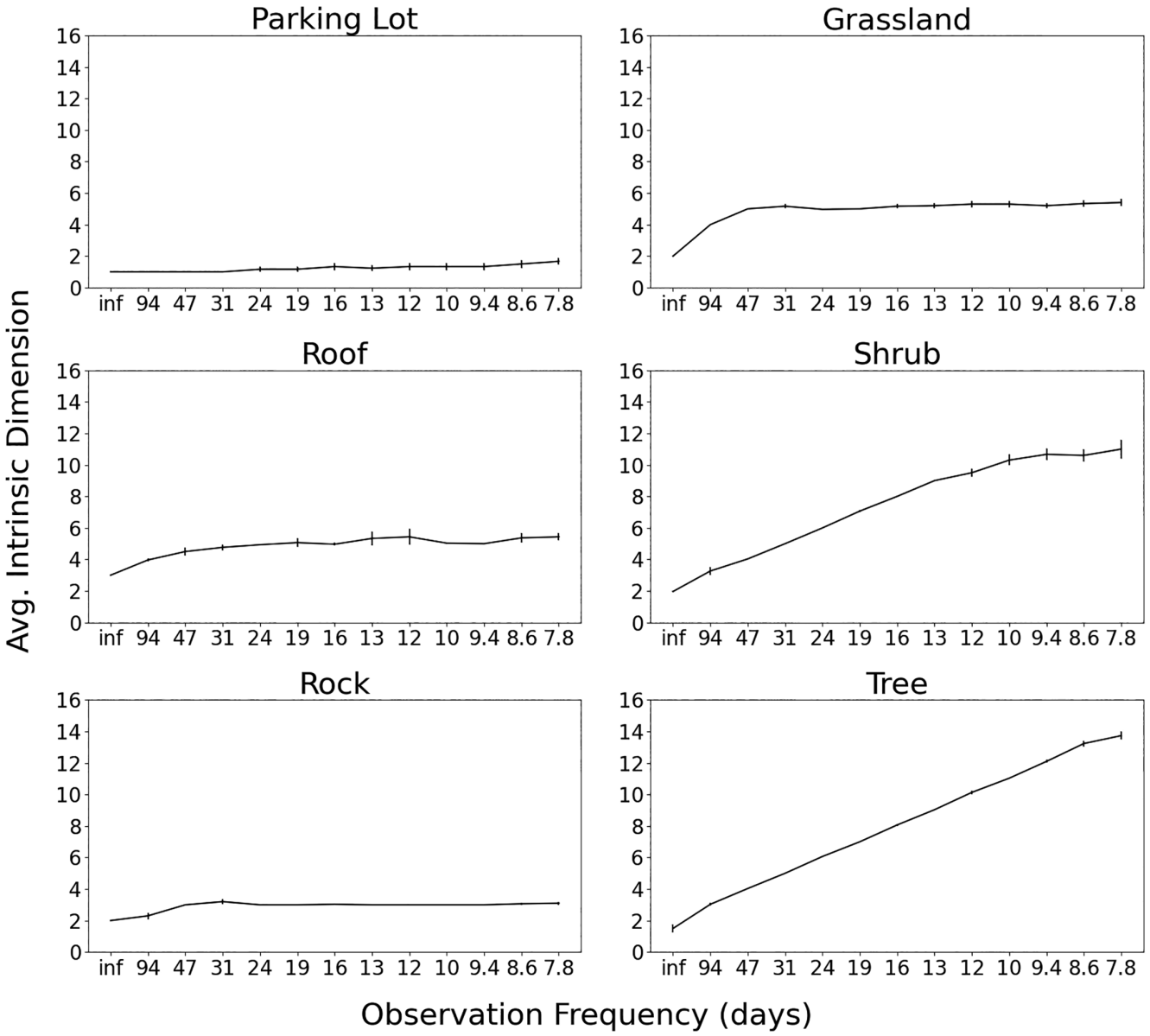

FIGURE 6 Temporal intrinsic dimensionality (ID) related to observation frequency. Each material had 500 pixels sampled with replacement for 30 batches, and the vertical lines represent the SD between batches. The frequencies evaluated include: Only a single observation (first observation; frequency = infinity); only the first and last observations (frequency = 94 days); the first, last, and center observations (frequency = 47 days), etc. Since the flights were not perfectly evenly spaced due to weather and flight constraints, the frequency is the average difference between the observations used.

replaces another species). This also means that true vegetation variability change, such as alien species overtaking diverse native plant populations, may be identifiable without needing to account for seasonal change. We consider spatial ID to be an index of vegetation variability, that is, it will illustrate a change, but further information will be required to determine what type of change has occurred. Thus, ID pairs well with other traditional methods of species detection, such as plant functional traits, etc.

The temporal ID study showed that the optimal revisit frequency for grasslands is ~monthly, for shrubs is ~10 days, and for trees is <7 days. During our observation period, the biochemical composition of trees changed rapidly, which manifests in significantly different spectral properties for each SHIFT revisit. This is consistent with the spectra shown by Chadwick et al. (2025). In addition, many vegetation changes, particularly in trees, are sudden/daily (e.g., spring bloom; deforestation), so even subweekly revisits may fail to capture these abrupt changes (Raiho et al., 2023). Cloud cover will also obscure many global observations (e.g., Ju & Roy, 2008), resulting in a larger effective revisit time to obtain

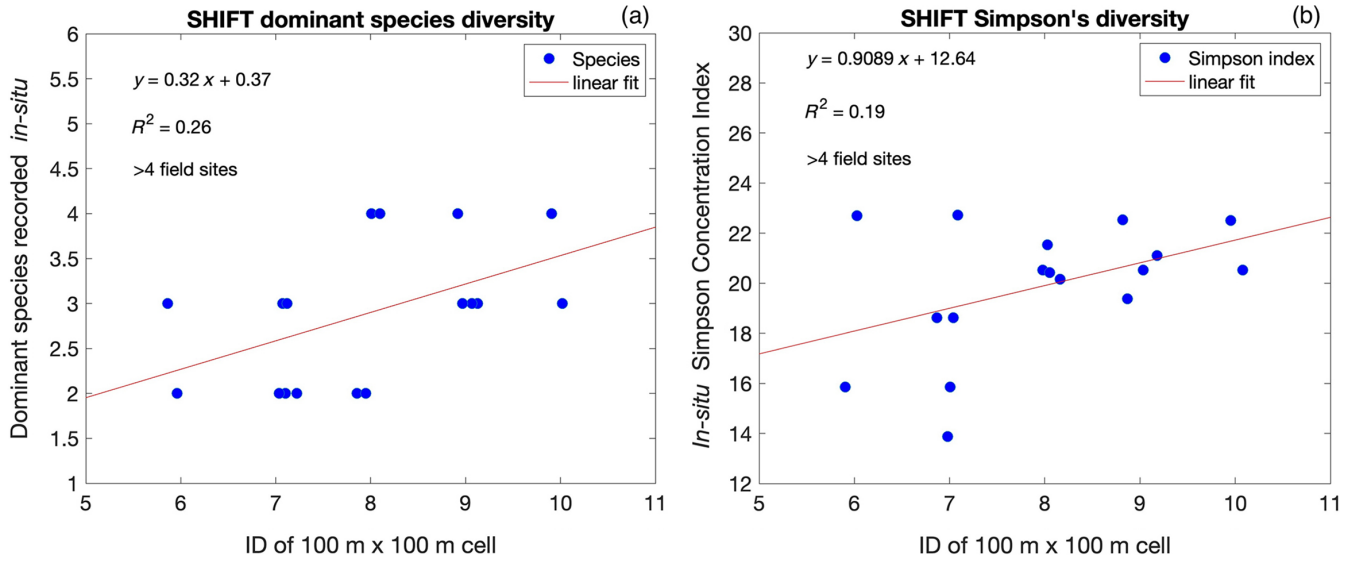

FIGURE 7 Spatial intrinsic dimensionality (ID) computed over a 100 m × 100 m cell is compared with (a) the number of recorded species with abundance >25% in each cell, and (b) the inverse Simpson concentration index. Due to the small area of each field plot (8 m × 8 m), field plots within 40 m of each cell center were combined, and 100 m × 100 m ID cells containing more than four field plots were used in the comparison to better represent the heterogeneity on the ground. Spatial ID is systematically higher than the number of dominant plot species recorded, which may be due to the larger spatial area considered, and also because some vegetation species may be difficult to identify in the field at certain times of year (particularly when senesced). A small amount of jitter is added to each point so that overlapping data values can be seen.

cloud-free imagery. Given the high beta diversity of the landscape, it is possible that the plot sampling has obscured some of the important biodiversity. For instance, grasslands are expected to change rapidly within a month, but ~weekly airborne observations may have aliased this. Similarly, many of the trees at Sedgwick and Dangermond are oaks, which may not change as significantly during a week. We believe that illumination and scattering also contributed to the increase in temporal ID (similarly for the shrubs).

In interpreting these findings from the material temporal ID study, it is crucial to acknowledge the inherent seasonal and climate dependencies of the data shown in Figure 6. Spatial ID inherently only captures canopy-emergent dominant species (i.e., not the understory vegetation), and some vegetation species may be difficult to identify in the field at certain times of year, particularly when senesced. The observed temporal patterns, particularly in the dynamic classes such as trees and shrubs, underscore the significance of long-term, multiannual studies across diverse geographical landscapes and the utility of remote sensing time series analysis for understanding these environments (Kennedy et al., 2014; Pasquarella et al., 2016). It is also remarkable that the algorithm works as well over a ~90-day period as it does during peak greenness. The stable classes (rock, parking lot, and roof) may no longer be spectrally stable under varying seasonal conditions or climate zones, and extended phenological changes in vegetation could significantly alter the observed ID patterns. Consequently, a comprehensive understanding necessitates expanding both the spatial and temporal domains to capture a broader array of climatic, geological, and seasonal contexts.

This is an important first study that evaluates spectral dimensionality across space and through time in a coastal region in a Mediterranean climate. The region of interest has a predominantly open canopy, which may differ fundamentally from closed canopy systems, such as tropical forests. In particular, the dense closed canopy may block understory species richness from being adequately observed by aerial imagery. The study should be repeated in other Mediterranean regions and in other bioclimatic regions to show that spectral ID–vegetation variability relationships are an intrinsic and quantifiable property. Spectral imagery acquired during NASA's BioSCape experiment in the Cape Floristic Region in South Africa will provide additional data against which to evaluate ID as a vegetation variability metric (Hestir et al., 2023).

CONCLUSION

We have proposed and evaluated ID as a method to quantify terrestrial vegetation variability. The SHIFT

airborne campaign provided an excellent test case with 13 near-weekly acquisitions over a three-month period, with coincident field acquisitions of plant species. Despite differences in spatial scales, our comparisons show encouraging correlation between spatial ID and in situ data. There is also very little variation in ID over the three-month period during which traditional vegetation metrics changed significantly, demonstrating robustness to seasonal change. Temporal ID, however, increased monotonically throughout the study, indicating the importance of frequent revisits and the value of harmonization between similar missions (such as synergies between SBG and the upcoming European Space Agency's Copernicus Hyperspectral Imaging Mission for the Environment—CHIME). ID does not require any training data and could be applied globally in this era of increasingly available imaging spectroscopy data. This has great potential for future spectroscopy missions such as SBG and CHIME, which could enable subseasonal global monitoring of plant diversity.

ACKNOWLEDGMENTS

We thank the Editor, reviewer Prof. Dan Sousa, and one other anonymous reviewer for their excellent feedback and suggestions, which led to significant improvements to this work. Support for K. Cawse-Nicholson, K.D. Chadwick, P.G. Brodrick, M. Kiper, D.R. Thompson, Z. Pierrat, D. Schimel, and C. Miller was provided by NASA and the Jet Propulsion Laboratory, California Institute of Technology. Specific supporting projects include the Surface Biology and Geology (SBG) mission, a NASA Earth Science Designated Observable, and BioSCape, supported by NASA grant 80NSSC21K0086, the National Research Foundation of South Africa (NRF), the South African Environmental Observation Network (SAEON), and the United Nations Educational, Scientific and Cultural Organization (UNESCO). Philip A. Townsend was supported by the NASA Surface Biology and Geology (SBG) project through JPL award 1673139 to the University of Wisconsin. Additional support to Philemon Tsele was provided by NSF ASCEND Biology Integration Institute (BII) award DBI 2021898. Support for Alexey N. Shiklomanov was provided by the SBG mission and the NASA Terrestrial Ecology and New (Early Career) Investigator programs. Zoe Amie Pierrat was supported by an appointment to the NASA Postdoctoral Program at the Jet Propulsion Laboratory, administered by Oak Ridge Associated Universities under contract with NASA. The research described in this paper was carried out at the Jet Propulsion Laboratory, California Institute of Technology, under contract with the National Aeronautics and Space Administration.

CONFLICT OF INTEREST STATEMENT

The authors declare no conflicts of interest.

DATA AVAILABILITY STATEMENT

AVIRIS-NG reflectance data (Brodrick et al., 2023) are available from https://daac.ornl.gov/cgi-bin/dsviewer.pl?ds_id=2183 with a full data description at https://daac.ornl.gov/SHIFT/guides/SHIFT_AVNG_L2A_RFL_unrec.html. SHIFT field data (Queally et al., 2024) are available from https://doi.org/10.3334/ORNLDAAC/2295. All code, noise estimates, and ID output (Cawse-Nicholson, 2025) are available from https://doi.org/10.5281/zenodo.14847832.

ORCID

Kerry Cawse-Nicholson https://orcid.org/0000-0002-0510-4066
K. Dana Chadwick https://orcid.org/0000-0002-5633-4865
Philip G. Brodrick https://orcid.org/0000-0001-9497-7661
Michael Kiper https://orcid.org/0009-0003-7282-0745
David R. Thompson https://orcid.org/0000-0003-1100-7550
David Schimel https://orcid.org/0000-0003-3473-8065
Charles E. Miller https://orcid.org/0000-0002-9380-4838
Philip A. Townsend https://orcid.org/0000-0001-7003-8774
Luciana F. Alves https://orcid.org/0000-0002-8944-1851
Alexey N. Shiklomanov https://orcid.org/0000-0003-4022-5979
Moses A. Cho https://orcid.org/0000-0003-4435-5375
Abel Ramoelo https://orcid.org/0000-0002-9917-9754
Philemon Tsele https://orcid.org/0000-0003-0765-7905
Nobuhle Majozi https://orcid.org/0000-0003-4592-4250
Zoe Amie Pierrat https://orcid.org/0000-0002-6726-2406
Simon Ferrier https://orcid.org/0000-0001-7884-2388

REFERENCES

Asner, G. P., D. E. Knapp, J. Boardman, R. O. Green, T. Kennedy-Bowdoin, M. Eastwood, and C. B. Field. 2012. "Carnegie Airborne Observatory-2: Increasing Science Data Dimensionality Via High-Fidelity Multi-Sensor Fusion." *Remote Sensing of Environment* 124: 454–465. https://doi.org/10.1016/j.rse.2012.06.012.

Bioucas-Dias, J. M., and J. M. Nascimento. 2008a. "Hyperspectral Subspace Identification." *IEEE Transactions on Geoscience and Remote Sensing* 46(8): 2435–45. https://doi.org/10.1109/TGRS.2008.918089.

Bioucas-Dias, J. M., and J. M. Nascimento. 2008b. "HySime (Hyperspectral Signal Subspace Identification by Minimum Error) MATLAB Code." http://www.lx.it.pt/~bioucas/code/demo_HySime.zip.

Bolnick, D. I., P. Amarasekare, M. S. Araújo, R. Bürger, J. M. Levine, M. Novak, and D. A. Vasseur. 2011. "Why Intraspecific Trait Variation Matters in Community Ecology." *Trends in Ecology & Evolution* 26(4): 183–192. https://doi.org/10.1016/j.tree.2011.01.009.

Brodrick, P., R. Pavlick, M. Bernas, J. W. Chapman, R. Eckert, M. Helmlinger, M. Hess-Flores, et al. 2023. "SHIFT: AVIRIS-NG L2A Unrectified Reflectance." ORNL DAAC, Oak Ridge, Tennessee, USA. [Dataset]. https://doi.org/10.3334/ORNLDAAC/2183.

Cavender-Bares, J., A. K. Schweiger, J. N. Pinto-Ledezma, and J. E. Meireles. 2020. "Applying Remote Sensing to Biodiversity Science." In *Remote Sensing of Plant Biodiversity*, edited by J. Cavender-Bares, J. A. Gamon, and P. A. Townsend, 23. Cham: Springer Nature. https://doi.org/10.1007/978-3-030-33157-3.

Cawse-Nicholson, K. 2025. "Intrinsic Dimensionality Zenodo Repository, Release v1.0-Shift." https://doi.org/10.5281/zenodo.14847832.

Cawse-Nicholson, K., S. Damelin, A. Robin, and M. Sears. 2013. "Determining the Intrinsic Dimension of a Hyperspectral Image Using Random Matrix Theory." *IEEE Transactions on Image Processing* 22(4): 1301–10. https://doi.org/10.1109/TIP.2012.2227765.

Cawse-Nicholson, K., S. J. Hook, C. E. Miller, and D. R. Thompson. 2019. "Intrinsic Dimensionality in Combined Visible to Thermal Infrared Imagery." *IEEE Journal of Selected Topics in Applied Earth Observations and Remote Sensing* 12(12): 4977–84. https://doi.org/10.1109/JSTARS.2019.2938883.

Cawse-Nicholson, K., A. M. Raiho, D. R. Thompson, G. C. Hulley, C. E. Miller, K. R. Miner, and S. K. Zareh. 2022. "Intrinsic Dimensionality as a Metric for the Impact of Mission Design Parameters." *Journal of Geophysical Research: Biogeosciences* 127(8): e2022JG006876. https://doi.org/10.1029/2022JG006876.

Cawse-Nicholson, K., A. M. Raiho, D. R. Thompson, G. C. Hulley, C. E. Miller, K. R. Miner, and S. K. Zareh. 2023. "Surface Biology and Geology Imaging Spectrometer: A Case Study to Optimize the Mission Design Using Intrinsic Dimensionality." *Remote Sensing of Environment* 290: 113534. https://doi.org/10.1016/j.rse.2023.113534.

Cawse-Nicholson, K., A. Robin, and M. Sears. 2013. "The Effect of Correlation on Determining the Intrinsic Dimension of a Hyperspectral Image." *IEEE Journal of Selected Topics in Applied Earth Observations and Remote Sensing* 6(2): 482–87. https://doi.org/10.1109/JSTARS.2013.2242847.

Cawse-Nicholson, K., P. A. Townsend, D. Schimel, A. M. Assiri, P. L. Blake, M. F. Buongiorno, and SBG Algorithms Working Group. 2021. "NASA's Surface Biology and Geology Designated Observable: A Perspective on Surface Imaging Algorithms." *Remote Sensing of Environment* 257: 112349. https://doi.org/10.1016/j.rse.2021.112349.

Chadwick, K. D., F. Davis, K. Miner, R. Pavlick, M. Reynolds, P. A. Townsend, P. G. Brodrick, et al. 2025. "Unlocking Ecological Insights from Sub-Seasonal Visible-to-Shortwave Infrared Imaging Spectroscopy: The SHIFT Campaign." *Ecosphere* 16(3): e70194. https://doi.org/10.1002/ecs2.70194.

Chao, A., N. J. Gotelli, T. C. Hsieh, E. L. Sander, K. H. Ma, R. K. Colwell, and A. M. Ellison. 2014. "Rarefaction and Extrapolation with Hill Numbers: A Framework for Sampling and Estimation in Species Diversity Studies." *Ecological Monographs* 84(1): 45–67. https://doi.org/10.1890/13-0133.1.

Cogliati, S., F. Sarti, L. Chiarantini, M. Cosi, R. Lorusso, E. Lopinto, and R. Colombo. 2021. "The PRISMA Imaging Spectroscopy Mission: Overview and First Performance Analysis." *Remote Sensing of Environment* 262: 112499. https://doi.org/10.1016/j.rse.2021.112499.

Draper, F. C., C. Baraloto, P. G. Brodrick, O. L. Phillips, R. V. Martinez, E. N. Honorio Coronado, T. R. Baker, et al. 2019. "Imaging Spectroscopy Predicts Variable Distance Decay across Contrasting Amazonian Tree Communities." *Journal of Ecology* 107: 696–710. https://doi.org/10.1111/1365-2745.13067.

Féret, J. B., and G. P. Asner. 2014. "Mapping Tropical Forest Canopy Diversity Using High-Fidelity Imaging Spectroscopy." *Ecological Applications* 24: 1289–96. https://doi.org/10.1890/13-1824.1.

Gholizadeh, H., J. A. Gamon, C. J. Helzer, and J. Cavender-Bares. 2020. "Multi-Temporal Assessment of Grassland α- and β-Diversity Using Hyperspectral Imaging." *Ecological Applications* 30(7): e02145. https://doi.org/10.1002/eap.2145.

Helsen, K., L. Bassi, H. Feilhauer, T. Kattenborn, H. Matsushima, E. Van Cleemput, and O. Honnay. 2021. "Evaluating Different Methods for Retrieving Intraspecific Leaf Trait Variation from Hyperspectral Leaf Reflectance." *Ecological Indicators* 130: 108111. https://doi.org/10.1016/j.ecolind.2021.108111.

Hestir, E. L., A. Wilson, A. Cardoso, J. Slingsby, and C. Forbes. 2023. "The NASA Biodiversity Survey of the Cape (BioSCape)." In *Optica Sensing Congress 2023 (AIS, FTS, HISE, Sensors, ES)*. Technical Digest Series, paper HM2C.3. Optica Publishing Group.

Heylen, R., M. Parente, and P. Gader. 2014. "A Review of Nonlinear Hyperspectral Unmixing Methods." *IEEE Journal of Selected Topics in Applied Earth Observations and Remote Sensing* 7(6): 1844–68. https://doi.org/10.1109/JSTARS.2014.2320576.

Ju, J., and D. P. Roy. 2008. "The Availability of Cloud-Free Landsat ETM+ Data over the Conterminous United States and Globally." *Remote Sensing of Environment* 112(3): 1196–1211. https://doi.org/10.1016/j.rse.2007.08.011.

Kennedy, R. E., S. Andréfouët, W. B. Cohen, C. Gómez, P. Griffiths, M. Hais, and Z. Zhu. 2014. "Bringing an Ecological View of Change to Landsat-Based Remote Sensing." *Frontiers in Ecology and the Environment* 12(6): 339–346. https://doi.org/10.1890/130066.

Kritchman, S., and B. Nadler. 2009. "Detection of the Number of Signals: Hypothesis Testing and Random Matrix Theory." *IEEE Transactions on Signal Processing* 57(10): 3930–41. https://doi.org/10.1109/TSP.2009.2022897.

Leitão, P. J., M. Schwieder, F. Pedroni, M. Sanchez, J. R. Pinto, L. Maracahipes, M. Bustamante, and P. Hostert. 2019. "Mapping Woody Plant Community Turnover with Space-Borne Hyperspectral Data–a Case Study in the Cerrado." *Remote Sensing in Ecology and Conservation* 5(1): 107–115. https://doi.org/10.1002/rse2.91.

Madonsela, S., M. A. Cho, A. Ramoelo, and O. Mutanga. 2017. "Remote Sensing of Species Diversity Using Landsat 8 Spectral Variables." *ISPRS Journal of Photogrammetry and Remote Sensing* 133: 116–127. https://doi.org/10.1016/j.isprsjprs.2017.10.008.

Madonsela, S., M. A. Cho, A. Ramoelo, and O. Mutanga. 2021. "Investigating the Relationship between Tree Species Diversity and Landsat-8 Spectral Heterogeneity across Multiple Phenological Stages." *Remote Sensing* 13(13): 2467. https://doi.org/10.1016/j.isprsjprs.2017.10.008.

Madonsela, S., M. A. Cho, A. Ramoelo, O. Mutanga, and L. Naidoo. 2018. "Estimating Tree Species Diversity in the Savannah Using NDVI and Woody Canopy Cover." *International Journal of Applied Earth Observation and Geoinformation* 66: 106–115. https://doi.org/10.1016/j.jag.2017.11.005.

Meer, P., J.-M. Jolion, and A. Rosenfeld. 1990. "A Fast Parallel Algorithm for Blind Estimation of Noise Variance." *IEEE Transactions on Pattern Analysis and Machine Intelligence* 12(3): 216–223. https://doi.org/10.1109/34.44408.

Millennium Ecosystem Assessment. 2005. "Ecosystems and Human Well-Being: Biodiversity Synthesis." http://www.millenniumassessment.org/documents/document.354.aspx.pdf.

Palmer, M. W., P. G. Earls, B. W. Hoagland, P. S. White, and T. Wohlgemuth. 2002. "Quantitative Tools for Perfecting Species Lists." *Environmetrics* 13(2): 121–137. https://doi.org/10.1002/env.516.

Palmer, M. W., T. Wohlgemuth, P. Earls, J. R. Arévalo, and S. Thompson. 2000. "Opportunities for Long-Term Ecological Research at the Tallgrass Prairie Preserve, Oklahoma." In *Cooperation in Long Term Ecological Research in Central and Eastern Europe. ILTER Regional Workshop, 22–25 June 1999, Budapest, Hungary*, edited by K. Lajtha and K. Vanderbilt, 123–28. Corvallis, OR: Oregon State University. https://andrewsforest.oregonstate.edu/sites/default/files/lter/pubs/pdf/pub2745.pdf.

Pasquarella, V. J., C. E. Holden, L. Kaufman, and C. E. Woodcock. 2016. "From Imagery to Ecology: Leveraging Time Series of all Available Landsat Observations to Map and Monitor Ecosystem State and Dynamics." *Remote Sensing in Ecology and Conservation* 2(3): 152–170. https://doi.org/10.1002/rse2.24.

Queally, N., F. W. Davis, K. D. Chadwick, C. Ade, L. Anderegg, Y. Angel, B. Baker, et al. 2024. *SHIFT: Vegetation Plot Characterization, Santa Barbara County, CA, 2022*. Oak Ridge, TN: ORNL DAAC. https://doi.org/10.3334/ORNLDAAC/2295.

Raiho, A. M., K. Cawse-Nicholson, A. Chlus, J. Dozier, M. Gierach, K. Miner, and B. Poulter. 2023. "Exploring Mission Design for Imaging Spectroscopy Retrievals for Land and Aquatic Ecosystems." *Journal of Geophysical Research: Biogeosciences* 128(4): e2022JG006833. https://doi.org/10.1029/2022JG006833.

Roberts, D. A., M. Gardner, R. Church, S. Ustin, G. Scheer, and R. O. Green. 1998. "Mapping Chaparral in the Santa Monica Mountains Using Multiple Endmember Spectral Mixture Models." *Remote Sensing of Environment* 65: 267–279. https://doi.org/10.1016/S0034-4257(98)00037-6.

Robin, A., K. Cawse-Nicholson, A. Mahmood, and M. Sears. 2015. "Estimation of the Intrinsic Dimension of Hyperspectral Images: Comparison of Current Methods." *IEEE Journal of Selected Topics in Applied Earth Observations and Remote Sensing* 8(6): 2854–61. https://doi.org/10.1109/JSTARS.2015.2432460.

Rocchini, D. 2007. "Effects of Spatial and Spectral Resolution in Estimating Ecosystem α-Diversity by Satellite Imagery." *Remote sensing of Environment* 111(4): 423–434. https://doi.org/10.1016/j.rse.2007.03.018.

Rossi, C., and H. Gholizadeh. 2023. "Uncovering the Hidden: Leveraging Sub-Pixel Spectral Diversity to Estimate Plant Diversity from Space." *Remote Sensing of Environment* 296: 113734. https://doi.org/10.1016/j.rse.2023.113734.

Sandel, B., C. Pavelka, T. Hayashi, L. Charles, J. Funk, F. W. Halliday, and M. J. Spasojevic. 2021. "Predicting Intraspecific Trait Variation among California's Grasses." *Journal of Ecology* 109(7): 2662–77. https://doi.org/10.1111/1365-2745.13673.

Schimel, D. S., G. P. Asner, and P. Moorcroft. 2013. "Observing Changing Ecological Diversity in the Anthropocene." *Frontiers in Ecology and the Environment* 11(3): 129–137. https://doi.org/10.1890/120111.

Schmidtlein, S., P. Zimmermann, R. Schüpferling, and C. Weiß. 2007. "Mapping the Floristic Continuum: Ordination Space Position Estimated from Imaging Spectroscopy." *Journal of Vegetation Science* 18: 131–140. https://doi.org/10.1111/j.1654-1103.2007.tb02523.x.

Schneider, F. D., F. Morsdorf, B. Schmid, O. L. Petchey, A. Hueni, D. S. Schimel, and M. E. Schaepman. 2017. "Mapping Functional Diversity from Remotely Sensed Morphological and Physiological Forest Traits." *Nature Communications* 8: 1441. https://doi.org/10.1038/s41467-017-01530-3.

Shannon, C. E. 1948. "A Mathematical Theory of Communication." *The Bell System Technical Journal* 27(3): 379–423. https://doi.org/10.1002/j.1538-7305.1948.tb01338.x.

Simpson, E. H. 1949. "Measurement of Diversity." *Nature* 163: 688. https://doi.org/10.1038/163688a0.

Singh, A., S. P. Serbin, B. E. McNeil, C. C. Kingdon, and P. A. Townsend. 2015. "Imaging Spectroscopy Algorithms for Mapping Canopy Foliar Chemical and Morphological Traits and their Uncertainties." *Ecological Applications* 25: 2180–97. https://doi.org/10.1890/14-2098.1.

Somers, B., G. P. Asner, L. Tits, and P. Coppin. 2011. "Endmember Variability in Spectral Mixture Analysis: A Review." *Remote Sensing of Environment* 115(7): 1603–16. https://doi.org/10.1016/j.rse.2011.03.003.

Sousa, D., P. Brodrick, K. Cawse-Nicholson, J. B. Fisher, R. Pavlick, C. Small, and D. R. Thompson. 2022. "The Spectral Mixture Residual: A Source of Low-Variance Information to Enhance the Explainability and Accuracy of Surface Biology and Geology Retrievals." *Journal of Geophysical Research: Biogeosciences* 127(2): e2021JG006672. https://doi.org/10.1029/2021JG006672.

Stavros, E. N., J. Chrone, K. Cawse-Nicholson, A. Freeman, N. F. Glenn, L. Guild, R. Kokaly, et al. 2023. "Designing an Observing System to Study the Surface Biology and Geology (SBG) of the Earth in the 2020s." *Journal of Geophysical Research: Biogeosciences* 128: e2021JG006471. https://doi.org/10.1029/2021JG006471.

Storch, T., H. P. Honold, S. Chabrillat, M. Habermeyer, P. Tucker, M. Brell, A. Ohndorf, et al. 2023. "The EnMAP Imaging Spectroscopy Mission towards Operations." *Remote Sensing of Environment* 294: 113632. https://doi.org/10.1016/j.rse.2023.113632.

Thompson, D. R., J. W. Boardman, M. L. Eastwood, and R. O. Green. 2017. "A Large Airborne Survey of Earth's Visible-Infrared Spectral Dimensionality." *Optics Express* 25: 9186–95. https://doi.org/10.1364/OE.25.009186.

Thompson, D. R., R. O. Green, C. Bradley, P. G. Brodrick, N. Mahowald, E. B. Dor, M. Bennett, et al. 2024. "On-Orbit Calibration and Performance of the EMIT Imaging Spectrometer." *Remote Sensing of Environment* 303: 113986. https://doi.org/10.1016/j.rse.2023.113986.

Thompson, D. R., V. Natraj, R. O. Green, M. C. Helmlinger, B. C. Gao, and M. L. Eastwood. 2018. "Optimal Estimation for Imaging Spectrometer Atmospheric Correction." *Remote Sensing of Environment* 216: 355–373. https://doi.org/10.1016/j.rse.2018.07.003.

United Nations Convention on Biological Diversity. 2020. "The Global Biodiversity Outlook 5 (GBO-5)." https://www.unep.org/resources/report/global-biodiversity-outlook-5-gbo-5.

United States Geological Survey. 2021. "NLCD 2021 Land Cover California Subset." https://data-cdfw.opendata.arcgis.com/content/CDFW::nlcd-2021-land-cover-california-subset.

Violle, C., B. J. Enquist, B. J. McGill, L. I. N. Jiang, C. H. Albert, C. Hulshof, and J. Messier. 2012. "The Return of the Variance: Intraspecific Variability in Community Ecology." *Trends in Ecology & Evolution* 27(4): 244–252. https://doi.org/10.1016/j.tree.2011.11.014.

Wang, R., and J. A. Gamon. 2019. "Remote Sensing of Terrestrial Plant Biodiversity." *Remote Sensing of Environment* 231: 111218. https://doi.org/10.1016/j.rse.2019.111218.

SUPPORTING INFORMATION

Additional supporting information can be found online in the Supporting Information section at the end of this article.

How to cite this article: Cawse-Nicholson, Kerry, K. Dana Chadwick, Philip G. Brodrick, Michael Kiper, David R. Thompson, David Schimel, Charles E. Miller, et al. 2025. "Intrinsic Dimensionality as a Metric for Temporal Plant Diversity Evaluation: Case Study from the SHIFT Campaign." *Ecosphere* 16(4): e70213. https://doi.org/10.1002/ecs2.70213